Homayonifar, M.; Mosler, J.:
Efficient modeling of microstructure evolution in magnesium by energy minimization
In: International Journal of Plasticity (2011) Elsevier

DOI: 10.1016/j.ijplas.2011.05.011

Efficient modeling of microstructure evolution in magnesium by energy minimization

Malek Homayonifar, Jörn Mosler

Helmholtz-Zentrum Geesthacht, Institute of Materials Research, Materials Mechanics, D-21502 Geesthacht, Germany

Abstract

The description of the complex interplay between deformation-induced twinning and dislocation slip, typical for metals showing an hcp structure such as magnesium, is of utmost importance for understanding their deformation behavior. In the present paper, an incremental energy principle is presented for that purpose. Within this principle, dislocation slip is modeled by crystal plasticity theory, while the phase decomposition associated with twinning is considered by a mixture theory. This mixture theory naturally avoids the decomposition of the twinning process into so-called *pseudo-dislocations* followed by a reorientation of the total crystal. By way of contrast, the proposed model captures the transformation of the crystal lattice due to twinning in a continuous fashion by simultaneously taking dislocation slip within both, possibly co-existent, phases into account. The shear strain induced by twinning as well as the deformation history are consistently included within the twinned domain by an enhanced multiplicative decomposition of the deformation gradient. Kinematic compatibility between the different phases is enforced by a Hadamard-type compatibility condition, while compatibility with respect to the boundary conditions requires the introduction of a boundary layer. The evolution of all state variables such as the twinning volume and the plastic strains associated with dislocation slip follow jointly and conveniently from minimizing the stress power of the total crystal. This canonical variational principle is closely related to the postulate of maximum dissipation and guarantees thermodynamical consistency of the resulting model. Particularly, the second law of thermodynamics is fulfilled. In sharp contrast to previous models suitable for the analysis of the deformation systems in magnesium, the Helmholtz energy of the twinning interfaces and that of the aforementioned boundary layer are considered. Analogously, the energy due to twinning nucleation and that related to twinning growth are accounted for by suitable dissipation functionals. By doing so, the number of twinning laminates becomes an additional unknown within the minimization principle and thus, the thickness of the lamellas can be computed. Interestingly, by interpreting this thickness as the mean free path of dislocations, a size effect of Hall-Petch-type can naturally be included within the novel model. The predictive capabilities of the resulting approach are finally demonstrated by analyzing the channel die test. For that purpose, a certain rank-two laminate structure is considered. However, it bears emphasis that the proposed framework is very general and consequently, it can also be applied to other materials.

Keywords: Deformation-induced twinning; magnesium; energy minimization; lamination theory

1. Introduction

Due to the high specific strength and its relatively low price, magnesium represents one of the most promising materials suitable for the design of light-weight structures, cf. Mordike and Ebert (2001). The only problems associated with that metal are related to its high corrosion activity and the comparably poor formability at room temperature. While the corrosion resistance of magnesium can be effectively improved either by a proper surface treatment or by alloying (see Blawert et al. (2008)), its formability is usually increased by conducting the respective forming process at elevated temperatures, typically at approximately 200° Celsius (see, e.g., Nebebe et al. (2009)). Clearly, from an economical point of view, lowering this temperature is desired. One important step necessary for achieving this goals is the understanding of the deformation systems in magnesium.

The deformation systems in magnesium are governed by its underlying hexagonal close-packed (hcp) atomic structure, cf. Christian and Mahajan (1995). This structure, combined with a lattice axial ratio of c/a=1.624, leads to a comparably small number of energetically favorable dislocation systems. One way for increasing this number, which is frequently observed in hcp metals such as magnesium (see Hauser et al. (1955); Reed-Hill and Robertson (1957); Yoshinaga and Horiuchi (1963); Tegart (1964); Wonsiewicz and Backofen (1967); Roberts and Partridge (1966); Obara et al. (1973); Lilleodden (2010) and Ando and Tonda (2000)), is given by deformation-induced twinning. This deformation mode yields a reoriented crystal lattice characterized by energetically more favorable dislocation systems. Accordingly, the overall mechanical response of magnesium is driven by a complex interplay between dislocation slip and deformation-induced twinning. Though some of the characteristic deformation modes in single crystal magnesium are reasonably well understood such that the basal systems $\langle 11\bar{2}0\rangle\{0001\}$ (Miller-Bravais indexing system for hcp lattices) and the prismatic systems $\langle 11\bar{2}0\rangle\{\bar{1}100\}$ are mostly responsible for plastic deformation, many questions are still open and controversially discussed in the literature, see Obara et al. (1973); Lilleodden (2010).

An effective method for analyzing the complex deformation systems in magnesium is provided by physically sound constitutive models. Such models have to capture deformation-induced twinning as well as dislocation slip. The latter is frequently modeled by crystal plasticity theory. This method was originally advocated in Rice (1971) and has been significantly further elaborated since then. A comprehensive recent overview of this constitutive description can be found, e.g., in Roters et al. (2010). Clearly, since crystal plasticity theory in its classical form does not account for deformation-induced twinning, the textures predicted by this theory are not in good agreement with those observed experimentally for materials showing an hcp lattice structure, see Agnew and Duygulu (2005); Khan et al. (2010).

Relatively straightforward approaches for incorporating deformation-induced twinning into classical crystal plasticity theory were proposed in Van Houtte (1978); Kalidindi (2001); Staroselsky and Anand (2003); Graff et al. (2007); Proust et al. (2009). Within such models, the shear strain induced by twinning is modeled by a so-called *pseudo dislocation*. If the respective strain reaches a certain threshold value, the crystal's orientation is rotated. Accordingly, the models proposed in the cited paper are based on a decomposition of the twinning history. Thus, simultaneous dislocation slip in both the initial phase and the twinning phase is not accounted for.

Alternatively, twinning can be modeled as a phase transformation or rather as a phase de-

composition. Such models go back to Ericksen (1979), see also James (1981); Kohn (1991). In sharp contrast to the approaches presented in Van Houtte (1978); Kalidindi (2001); Staroselsky and Anand (2003); Graff et al. (2007); Proust et al. (2009), this concept allows to consider the deformation systems in both phases simultaneously – as observed in experiments. Equally importantly, the deformation in such phases can be different. For guaranteeing continuity of the total deformation, Hadamard-like compatibility conditions are enforced, cf. Pitteri (1985); Ball and James (1987). Mathematically speaking, the modeling of twinning as phase decomposition can be interpreted as a certain rank-one convexification, cf. Ortiz and Repetto (1999); Carstensen et al. (2002). While the aforementioned modeling approach has been frequently applied to the martensitic phase transformation occurring in shape memory alloys (see Ball and James (1987); Simha (1997); Mueller (1999); Idesman et al. (2000); James and Hane (2000); Mielke et al. (2002); Aubry and Ortiz (2003)), it has only been rarely considered for the description of deformation-induced twinning. Scarce counterexamples are given by Kochmann and Le (2008, 2009) and Homayonifar and Mosler (2010). While in Kochmann and Le (2008, 2009) a very simple mechanical prototype model was analyzed, the method advocated in Homayonifar and Mosler (2010) does capture the most relevant deformation systems in magnesium. However, although the constitutive framework discussed in Homayonifar and Mosler (2010) is motivated by the theory of phase decomposition, the final model is again based on a decomposition of the twinning history into pseudo-dislocations followed by a reorientation of the total crystal. Consequently, simultaneous dislocation slip within both co-existent phases is not accounted for.

In the present paper, the concept of phase decomposition is combined with that of crystal plasticity theory leading to a consistent description of the deformation systems in magnesium. For that purpose and in line with Carstensen et al. (2002); Miehe and Lambrecht (2003); Mosler and Bruhns (2009b); Homayonifar and Mosler (2010), a variational principle is developed. This principle allows to compute all unknowns such as the plastic slip associated with dislocations and the reorientation of the crystal lattice due to twinning based on minimizing the stress power. In addition to its physical and mathematical elegance, this variational method shows several further advantages compared to conventional approaches, cf. Mosler and Bruhns (2009b). One of such advantages which is very important here is that energy minimization leads to a natural coupling of deformation-induced twinning and dislocation slip, i.e., that combination between such mechanisms is chosen which is energetically most favorable. This feature has already been used for analyzing the interplay between plastic deformation and wrinkling in membranes, cf. Mosler and Cirak (2009). Equally importantly, the framework of energy optimization opens up the possibility of studying also the subgrain microstructure of crystals such as that related to dislocations, see Ortiz and Repetto (1999); Carstensen et al. (2002); Kochmann and Le (2008); Hansen et al. (2010). It is noteworthy that the evolution of the microstructure predicted by such models is in remarkably good agreement with that observed in experiments, see Rasmussen and Pedersen (1980); Ortiz and Repetto (1999).

Similar to Ortiz and Repetto (1999); Carstensen et al. (2002); Kochmann and Le (2008); Hansen et al. (2010), the subgrain microstructure in magnesium is approximated by certain laminates in the present paper. Furthermore and analogously to Hansen et al. (2010), a so-called *boundary layer* necessary for fulfilling the boundary conditions at the microstructure is introduced. However, and in sharp contrast to Hansen et al. (2010) where the subgrain dislocation structure in FCC metals has been investigated, a novel constitutive model suitable for the analysis

of magnesium is elaborated in the present paper. For that purpose, a physically sound Helmholtz energy for the twinning interfaces and an additional one for the aforementioned boundary layer are proposed. Analogously, suitable dissipation functionals related to twinning nucleation and twinning growth are elaborated. By doing so, the number of twinning laminates becomes an additional unknown within the minimization principle and thus, the thickness of the lamellas can be computed. Interestingly, by interpreting this thickness as the mean free path of dislocations, a size effect of Hall-Petch-type can naturally be included within the novel model, cf. Aubry and Ortiz (2003).

One question which is open and currently under debate in the scientific literature is how a dislocation is altered when a twinning interface moves across it, cf. Kim et al. (2009). This question is also important for the model advocated in the present paper. Physically speaking, when twinning leads to a new phase, proper initial conditions for the dislocation structure have to be chosen. One possible assumption would be that the deformation history is completely reset by twinning. Alternatively, one could assume that the dislocation structures is not at all affected by twinning. For describing the deformation history of the new phase and for providing enough flexibility, an enhanced multiplicative decomposition of the deformation gradient is considered, cf. Boyce et al. (1992); Levitas (1998); Idesman et al. (2000); Lion (2000); Meggyes (2001). The respective kinematics accounts consistently for the initial structure and the evolution of the dislocations within the new phase, the deformation due to twinning as well as for the elastic lattice distortion.

The paper is organized as follows: Section 2 is concerned with the crystal plasticity theory and its variationally consistent reformulation. Within the resulting model all unknown slip rates follow naturally from minimizing the stress power. The probably most important novel contributions can be found in Section 3. Within this section, a physically sound model suitable for the analysis of deformation-induced twinning is elaborated. Starting from an approximation of the underlying kinematics based on lamination theory, the constitutive assumptions are subsequently discussed. The predictive capabilities of the novel model are finally demonstrated in Section 4. For that purpose, the channel die test introduced in Kelley and Hosford (1968) is numerically analyzed.

2. Variationally consistent crystal plasticity theory

This section is associated with the modeling of dislocation slip in magnesium resulting from dislocations. Deformation-induced twinning is excluded here. For describing dislocation slip, a model falling into the range of crystal plasticity theory is considered. Following Ortiz and Stainier (1999), this model is recast into a variationally consistent format which allows to compute all state variables, together with the unknown deformation, jointly and conveniently by minimizing an incrementally defined energy functional. Although this approach has already been published in Homayonifar and Mosler (2010), this section cannot be removed for two reasons. First, it serves for introducing the notations used within the present paper. Secondly and equally importantly, the final novel model suitable for the analysis of interacting dislocation slip and deformation-induced twinning relies, among others, on precisely the aforementioned crystal plasticity framework. The present section follows to a large extend Homayonifar and Mosler (2010). However, a more concise format is chosen here.

2.1. Fundamentals of crystal plasticity theory – In a nutshell

The fundamentals of crystal plasticity theory are introduced here. Since they are nowadays well known, they are simply summarized in Tab. 1. The mechanical response implied by such assumptions can be derived in standard manner. More precisely, applying the by now classical Coleman & Noll procedure (see Coleman (1964)) to the dissipation inequality

$$\mathcal{D} = \boldsymbol{P} : \dot{\boldsymbol{F}} - \dot{\Psi} \geq 0 \tag{8}$$

and considering elastic processes, yields the second Piola-Kirchhoff stress tensor

$$\boldsymbol{S} = 2\frac{\partial \Psi}{\partial \boldsymbol{C}} = 2(\boldsymbol{F}^{\mathrm{p}})^{-1} \cdot \frac{\partial \Psi}{\partial \boldsymbol{C}^{\mathrm{e}}} \cdot (\boldsymbol{F}^{\mathrm{p}})^{-\mathrm{T}} \tag{9}$$

and subsequently, the Mandel stresses $\boldsymbol{\Sigma} := 2\boldsymbol{C}^{\mathrm{e}} \cdot \partial_{\boldsymbol{C}^{\mathrm{e}}} \Psi^{\mathrm{e}}$, cf. (Mandel, 1972). In Eq. (8), $\boldsymbol{P}$ denotes the first Piola-Kirchhoff stress tensor and thus, the product $\boldsymbol{P} : \dot{\boldsymbol{F}}$ is the stress power. Focusing now on an inelastic deformation, inserting Eq. (9) into the dissipation inequality (8), together with the degree-one positive homogeneity of the yield function, results in the reduced dissipation inequality

$$\mathcal{D} \overset{\phi^a=0}{=} \sum_{a=1}^{n} \zeta^{(a)} \, \Sigma_0^{(a)} \geq 0. \tag{10}$$

Since the initial yield stress is always positive ($\Sigma_0^{(a)} > 0$) and the plastic multiplier is non-negative ($\zeta^{(a)} \geq 0$), the second law of thermodynamics is indeed fulfilled by the constitutive framework summarized in Tab. 1. Equally importantly, Eq. (10) allows to compute the dissipation in closed form. Furthermore, since $\Sigma_0^{(a)} = \text{const}$, the dissipation can be integrated analytically in time. This is particularly convenient for the variational constitutive updates discussed next.

2.2. A variational reformulation of crystal plasticity theory

In this subsection, the crystal plasticity model addressed before is reformulated into a variationally consistent framework. Within this framework all state variables, together with the unknown deformation of the considered solid, follow jointly and conveniently from minimizing an incrementally defined potential, cf. Ortiz and Stainier (1999); Miehe (2002); Carstensen et al. (2002); Mosler and Bruhns (2009a,b). For rate-independent processes which are in the focus of attention, this potential turns out to be the stress power. In addition to the mathematical and physical elegance, the aforementioned variational formulations show several further advantages compared to conventional approaches, cf. Mosler and Bruhns (2009b). The one which is probably most important within the present paper is that energy principles provide a physically sound basis for coupling different models, cf. Mosler and Cirak (2009), i.e., the energetically most favorable combination between the respective models is considered. Such a canonical coupling is also proposed in the present paper for combining dislocation slip and deformation-induced twinning.

As mentioned before, the stress power plays an important role within the variational reformulation of crystal plasticity theory. Following Ortiz and Stainier (1999); Mosler and Bruhns (2009b), it can be written as

$$\mathcal{E}(\dot{\boldsymbol{\varphi}}, \zeta^{(1)}, \ldots, \zeta^{(n)}) = \dot{\Psi}(\dot{\boldsymbol{\varphi}}, \zeta^{(1)}, \ldots, \zeta^{(n)}) + \mathcal{D}(\zeta^{(1)}, \ldots, \zeta^{(n)}) \tag{11}$$

- Multiplicative decomposition of the deformation gradient $\boldsymbol{F}$

$$\boldsymbol{F} = \boldsymbol{F}^{\mathrm{e}} \cdot \boldsymbol{F}^{\mathrm{p}} \;\text{ with }\; \det(\boldsymbol{F}^{\mathrm{e}}) > 0 \text{ and } \det(\boldsymbol{F}^{\mathrm{p}}) > 0 \tag{1}$$

  Here, $\boldsymbol{F}^{\mathrm{e}}$ is associated with elastic and $\boldsymbol{F}^{\mathrm{p}}$ with plastic deformations, cf. Lee (1969).

- Additive decomposition of the Helmholtz energy Ψ

$$\Psi = \Psi^{\mathrm{e}}(\boldsymbol{C}^{\mathrm{e}}) + \Psi^{\mathrm{p}}(\boldsymbol{\lambda}), \quad \text{with} \quad \boldsymbol{C}^{\mathrm{e}} := \boldsymbol{F}^{\mathrm{e}T} \cdot \boldsymbol{F}^{\mathrm{e}}, \quad \boldsymbol{\lambda} = \{\lambda^{(1)}, \ldots, \lambda^{(n)}\} \tag{2}$$

  In Eq. (2), Ψ^{e} defines the mechanical response to fully reversible deformations, while Ψ^{p} is related to plastic work. $\lambda^{(a)}$ is a strain-like internal variable governing isotropic hardening of slip system a.

- Additive decomposition of the Helmholtz energy into self and latent hardening

$$\Psi^{\mathrm{p}} = \Psi^{\mathrm{p}}_{\mathrm{self}} + \Psi^{\mathrm{p}}_{\mathrm{lat}} \tag{3}$$

- Definition of the space of admissible stresses $\mathbb{E}_{\boldsymbol{\sigma}}$

$$\mathbb{E}_{\boldsymbol{\sigma}} = \left\{ (\boldsymbol{\Sigma}, \boldsymbol{Q}) \in \mathbb{R}^{9+n} \;\middle|\; \phi^{(a)}(\boldsymbol{\Sigma}, Q^{(a)}) \leq 0,\ a = 1, ..., n \right\} \tag{4}$$

  by means of n convex yield functions $\phi^{(a)}$ of Schmid-type, i.e.,

$$\phi^{(a)}(\boldsymbol{\Sigma}, \boldsymbol{\lambda}) = |\boldsymbol{\Sigma} : \boldsymbol{N}^{(a)}| - (\Sigma_0^{(a)} - Q^{(a)}(\boldsymbol{\lambda})), \quad Q^{(a)} = -\partial_{\lambda^{(a)}} \Psi^{\mathrm{p}} \tag{5}$$

  Here, $\boldsymbol{N}^{(a)} := (\boldsymbol{s}^{(a)} \otimes \boldsymbol{m}^{(a)})$ is the Schmid tensor defined by the orthogonal unit vectors $\boldsymbol{m}^{(a)}$ and $\boldsymbol{s}^{(a)}$, $\boldsymbol{\Sigma}$ is the Mandel stress tensor, $\Sigma_0^{(a)}$ is the initial yield stress and the stress-like internal variable $Q^{(a)}$ conjugate to $\lambda^{(a)}$ governs isotropic hardening of slip system a.

- Associative evolution equations (postulate of maximum dissipation, cf. Hill (1972))

$$\boldsymbol{l}^{\mathrm{p}} := \dot{\boldsymbol{F}}^{\mathrm{p}} \cdot \boldsymbol{F}^{\mathrm{p}-1} = \sum_{a=1}^{n} \zeta^{(a)} \operatorname{sign}[\boldsymbol{\Sigma} : \boldsymbol{N}^{(a)}]\, \boldsymbol{N}^{(a)} \quad \text{and} \quad \dot{\lambda}^a = \zeta^{(a)} \frac{\partial \phi^{(a)}}{\partial Q^{(a)}} = \zeta^{(a)} \tag{6}$$

  Here, $\zeta^{(a)}$ denotes the plastic multiplier related to slip system a and the superposed dote is the material time derivative.

- Karush-Kuhn-Tucker optimality conditions

$$\zeta^{(a)} \geq 0\ ,\ \zeta^{(a)}\ \dot{\phi}^{(a)} = 0 \tag{7}$$

Table 1: Summary of the constitutive equations defining the crystal plasticity model used within the present paper

for physically admissible states. If energy minimization is the overriding principle, inadmissible states can simply be excluded by considering the constrained functional

$$\mathcal{E} = \begin{cases} \dot{\Psi}(\dot{\boldsymbol{\varphi}}, \zeta^{(1)}, \dots, \zeta^{(n)}) + \mathcal{D}(\zeta^{(1)}, \dots, \zeta^{(n)}) & \forall \text{ admissible states} \\ \infty & \text{otherwise.} \end{cases} \tag{12}$$

It bears emphasis that the associative low rule $(6)_1$ and the evolution equations $(6)_2$ are already included in Eqs. (11) and (12). As a consequence, the dissipation $\mathcal{D}$ is given by Eq. (10). The interesting properties of functionals (11) or (12) become evident, if their stationarity conditions are computed. By inserting Eq. (10) into Eq. (11) and considering the identities

$$\dot{\boldsymbol{F}}^{\mathrm{e}}(\dot{\boldsymbol{F}}, \dot{\boldsymbol{F}}^{\mathrm{p}})|_{\dot{\boldsymbol{F}}=\boldsymbol{0}} = -\sum_{a=1}^{n} \zeta^{(a)} \operatorname{sign}[\boldsymbol{\Sigma} : \boldsymbol{N}^{(a)}] \; \boldsymbol{F}^{\mathrm{e}} \cdot \boldsymbol{N}^{(a)}, \quad \dot{\boldsymbol{F}}^{\mathrm{e}}(\dot{\boldsymbol{F}}, \dot{\boldsymbol{F}}^{\mathrm{p}})|_{\dot{\boldsymbol{F}}^{\mathrm{p}}=\boldsymbol{0}} = \dot{\boldsymbol{F}} \cdot \boldsymbol{F}^{\mathrm{p}-1}, \tag{13}$$

together with the homogeneity of the yield function, the stress power $\mathcal{E}$ can finally be re-written as

$$\begin{aligned} \mathcal{E} &= \boldsymbol{P} : \dot{\boldsymbol{F}} - \sum_{a=1}^{n} \zeta^{(a)} \; |\boldsymbol{\Sigma} : \boldsymbol{N}^{(a)}| - \sum_{a=1}^{n} \zeta^{(a)} \; Q^{(a)} + \sum_{a=1}^{n} \zeta^{(a)} \; \Sigma_0^{(a)} \\ &= \boldsymbol{P} : \dot{\boldsymbol{F}} - \sum_{a=1}^{n} \zeta^{(a)} \phi^{(a)}. \end{aligned} \tag{14}$$

Accordingly, stability of Eq. (14) with respect to the plastic multiplier $\zeta^{(a)}$ yields

$$\frac{\partial \mathcal{E}}{\partial \zeta^{(a)}} = -\phi^{(a)} \geq 0. \tag{15}$$

Thus, energy minimization of $\mathcal{E}$ predicts plastic multipliers fully equivalent to those of the conventional plasticity model discussed in the previous subsection. As a result,

$$(\zeta^{(1)}, \dots, \zeta^{(n)}) = \arg\inf \mathcal{E}(\dot{\boldsymbol{\varphi}}, \zeta^{(1)}, \dots, \zeta^{(n)})\big|_{\dot{\boldsymbol{\varphi}}=\text{const}} \tag{16}$$

represents indeed a variationally consistent reformulation of the crystal plasticity model summarized in Tab. 1. Furthermore, it defines the reduced potential

$$\mathcal{E}_{\mathrm{red}} = \inf_{\zeta^{(1)}, \dots, \zeta^{(n)}} \mathcal{E}(\dot{\boldsymbol{\varphi}}, \zeta^{(1)}, \dots, \zeta^{(n)}). \tag{17}$$

Taking the Karush-Kuhn-Tucker optimality conditions (7) into account, this reduced potential is simply the stress power (see Eq. (14))

$$\mathcal{E}_{\mathrm{red}} = \boldsymbol{P} : \dot{\boldsymbol{F}}. \tag{18}$$

Consequently, $\mathcal{E}_{\mathrm{red}}$ acts like a hyperelastic potential, i.e., the stresses are conveniently derived from

$$\boldsymbol{P} = \frac{\partial \mathcal{E}_{\mathrm{red}}}{\partial \dot{\boldsymbol{F}}}. \tag{19}$$

Further details on variational constitutive updates are omitted here. They can be found, e.g., in Ortiz and Stainier (1999); Miehe (2002); Carstensen et al. (2002); Mosler and Bruhns (2009a,b).

Remark 1. *In case of rate-independent plasticity theory, the dissipation is a positively homogeneous function of degree one, cf. Ortiz and Stainier (1999); Hackl and Fischer (2008) (see also Eq. (10)). In the present paper, it followed from a Legendre-Fenchel transformation applied to the characteristic function of the space of admissible stresses, see Mosler and Bruhns (2009a); Homayonifar and Mosler (2010). Thus, it depends on the underlying yield function representing the primary assumption. By way of contrast, the dissipation and the flow rule represent the primary variables in Ortiz and Stainier (1999); Ortiz and Repetto (1999) and the yield function is derived from them. Both methods are connected through a Legendre-Fenchel transformation. Therefore, they are essentially equivalent for rate-independent processes. However, depending on the application, one of these methods can be advantageous. For instance, the approach advocated in Ortiz and Stainier (1999); Ortiz and Repetto (1999) will be chosen for elaborating the model suitable for the analysis of deformation-induced twinning.*

2.3. Numerical implementation - Variational constitutive updates

An additional advantage of the variationally consistent formulation of crystal plasticity concisely summarized in the previous subsection, is its naturally implied numerical implementation, cf. Ortiz and Stainier (1999); Miehe (2002); Carstensen et al. (2002); Mosler and Bruhns (2009a,b). More specifically, by considering a time integration over the interval $t \in [t_n; t_{n+1}]$, the continuously defined potential (11) is transformed into the discrete counterpart

$$I_{\text{inc}} = \int_{t_n}^{t_{n+1}} \mathcal{E} \, \mathrm{d}t = \Psi_{n+1} - \Psi_n + \sum_{a=1}^{n} \Delta\zeta^{(a)} \, \Sigma_0^{(a)}, \quad \Delta\zeta^{(a)} := \int_{t_n}^{t_{n+1}} \zeta^{(a)} \, \mathrm{d}t. \tag{20}$$

Since the dissipation depends linearly in the scalar-valued plastic multipliers $\zeta^{(a)}$, it can be integrated analytically. The same holds for the internal variables ($\lambda_{n+1}^{(a)} = \lambda_n^{(a)} + \Delta\zeta^{(a)}$). By way of contrast, the highly nonlinear Helmholtz energy requires an approximation of the time integration. Here, an exponential integration scheme is adopted for the plastic part of the deformation gradient, i.e.,

$$\boldsymbol{F}_{n+1}^{\text{p}} = \exp\left[\sum_{a=1}^{n} \Delta\zeta^{(a)} \, \text{sign}[\boldsymbol{\Sigma} : \boldsymbol{N}^{(a)}] \, \boldsymbol{N}^{(a)}\right] \cdot \boldsymbol{F}_n^{\text{p}} \tag{21}$$

Inserting this approximation into Eq. (20), yields finally

$$I_{\text{inc}} = I_{\text{inc}}(\boldsymbol{F}_{n+1}, \Delta\zeta^{(1)}, \ldots, \Delta\zeta^{(n)}). \tag{22}$$

Fully analogously to the continuous case, the slip rates can be computed from this potential according to

$$(\Delta\zeta^{(1)}, \ldots, \Delta\zeta^{(n)}) = \arg \inf_{\Delta\zeta^{(1)}, \ldots, \Delta\zeta^{(n)}} I_{\text{inc}}|_{\boldsymbol{F}_{n+1}} \tag{23}$$

and finally, the stresses are derived from

$$\boldsymbol{P} = \partial_{\boldsymbol{F}_{n+1}} \inf_{\Delta\zeta^{(1)}, \ldots, \Delta\zeta^{(n)}} I_{\text{inc}}, \tag{24}$$

cf. Homayonifar and Mosler (2010).

Remark 2. *Evidently, potential I_{inc} depends on the underlying time integration for $\boldsymbol{F}^{\mathrm{p}}$. Therefore, the discrete solution, i.e., $\Delta\zeta^{(1)},\ldots,\Delta\zeta^{(n)}$, depends on this integration scheme as well. However, it can be proved in a straightforward manner, that any consistent time integration scheme fulfilling*

$$\lim_{\Delta t\to 0} \boldsymbol{F}^{\mathrm{p}}_{n+1} - \boldsymbol{F}^{\mathrm{p}}_{n} = \boldsymbol{0}, \quad \lim_{\Delta t\to 0} \frac{\boldsymbol{F}^{\mathrm{p}}_{n+1} - \boldsymbol{F}^{\mathrm{p}}_{n}}{t_{n+1}-t_n} = \dot{\boldsymbol{F}}^{\mathrm{p}} \tag{25}$$

results in a consistent approximation of the continuous optimization problem, i.e.,

$$(\zeta^{(1)},\ldots,\zeta 6^{(n)}) = \lim_{\Delta t\to 0}\left[\frac{\arg\inf_{\Delta\zeta^{(1)},\ldots,\Delta\zeta^{(n)}} I_{\mathrm{inc}}|_{\boldsymbol{F}_{n+1}}}{t_{n+1}-t_n}\right]. \tag{26}$$

Further details are omitted here. They can be found, e.g., in Mosler and Bruhns (2009a,b).

2.4. Numerical analysis of the channel die test for a sample showing only pyramidal slip

The material parameters of the crystal plasticity model discussed before are calibrated here. For that purpose, an experiment is considered in which deformation-induced twinning is not observed. One such experiment is the channel die test, cf. Kelley and Hosford (1968) (see also Homayonifar and Mosler (2010); Graff et al. (2007)). For this experiment, the sample labeled as "A" in Kelley and Hosford (1968), is chosen. For this orientation, only pyramidal dislocations ($\{[2\bar{1}\bar{1}\bar{3}](2\bar{1}\bar{1}2)$, $[2\bar{1}\bar{1}3](\bar{2}112)\}$) can form. Since these dislocations are energetically equivalent and symmetric, their induced plastic deformation is a pure stretch (no macroscopic shear).

The macroscopic deformation characterizing the channel die test can be conveniently approximated by a plane strain field of the type

$$\boldsymbol{F} = \boldsymbol{I} - \varepsilon(\boldsymbol{e}_3\otimes\boldsymbol{e}_3) + \tilde{\varepsilon}(\boldsymbol{e}_1\otimes\boldsymbol{e}_1). \tag{27}$$

Here, ε and $\tilde{\varepsilon}$ are the compression and extension strain in the punching direction ($\boldsymbol{e}_3$) and in the channel direction ($\boldsymbol{e}_1$). Due to elastic deformation, the macroscopic deformation is usually not purely isochoric. Accordingly, $\tilde{\varepsilon}$ is not necessarily identical to $1/\varepsilon$.

Although the elastic deformation can be considered as small, a Helmholtz energy suitable for large strain effects is chosen. It is given by

$$\Psi^{\mathrm{e}}(\boldsymbol{C}^{\mathrm{e}}) = \frac{\lambda_{\mathrm{E}}}{2}(\ln(J^{\mathrm{e}}))^2 - \mu\ln(J^{\mathrm{e}}) + \frac{\mu}{2}(\mathrm{tr}(\boldsymbol{C}^{\mathrm{e}})-3). \tag{28}$$

In Eq. (28), J^{e} is the determinant of the elastic deformation gradient and $\{\lambda_{\mathrm{E}},\mu\}$ are the Lamé constants. Since, the macroscopic elastic anisotropy of magnesium is not very pronounced, an isotropic model such as that defined by Eq. (28) represents a suitable choice. However, a more complex anisotropic model could also be applied. It would not require any significant modification of the proposed framework.

The Helmholtz energy is completed by choosing a suitable hardening model. According to Kelley and Hosford (1968), the mechanical response of pyramidal slip systems can be reasonably approximated by an exponential hardening law. For this reason,

$$Q^{(a)}_{\mathrm{self}} = -\frac{\partial\Psi^{\mathrm{p}}_{\mathrm{self}}}{\partial\lambda^{(a)}} = \Sigma_\infty(1-\exp(-h_0\lambda^{(a)}/\Sigma_\infty)) \tag{29}$$

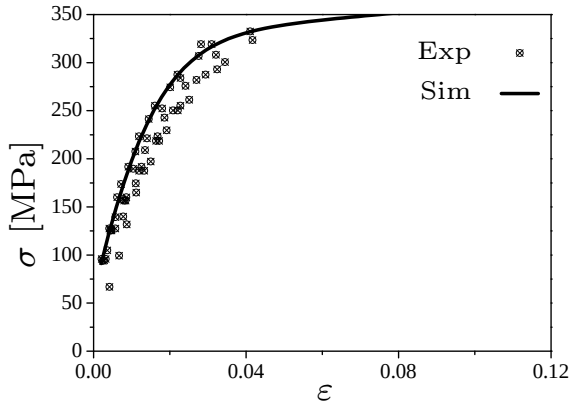

Elastic Properties	$\lambda_E = 34$(GPa)		μ =17 (GPa)	
Hardening parameters				
	Σ_0 (MPa)	h_0 (MPa)	Σ_∞ (MPa)	l^{ab}
Pyramidal	25	7100	105	25

Figure 1: Channel die test: left: comparison between experimentally measured stress-strain response (see Kelley and Hosford (1968); sample A) and numerical simulation; right: material parameters used within the computation

is considered with h_0 and Σ_∞ being material parameters. By way of contrast, less information is available for latent hardening. Consequently, a linear model characterized by a quadratic energy

$$\Psi^{\mathrm{p}}_{\mathrm{lat}} = \frac{1}{2}\,\boldsymbol{\lambda}\cdot\boldsymbol{l}\cdot\boldsymbol{\lambda}. \tag{30}$$

is employed. Hence, the resulting hardening moduli

$$l^{ab} := \frac{\partial^2 \Psi^{\mathrm{p}}_{\mathrm{lat}}}{\partial\lambda^{(a)}\partial\lambda^{(b)}} \tag{31}$$

are constant.

The parameters of the presented constitutive model were computed by comparing the experimentally observed mechanical response (see Kelley and Hosford (1968)) to its numerical counterpart. The results are shown in Fig. 1. Accordingly, the stress-strain response predicted by the crystal plasticity model combined with the material parameters in Fig. 1 shows a good agreement with the experimentally observed data.

3. Modeling deformation-induced twinning

The crystal plasticity model introduced before captures the mechanical response associated with dislocation slip in magnesium. However, that model does not capture the important effects of deformation-induced twinning frequently observed in metals showing an hcp lattice structure such as magnesium plays also an important role. For this reason, a novel model suitable for the analysis of this deformation mode is elaborated here and finally combined with the crystal plasticity model. Following the previous section, a variationally consistent framework is advocated, i.e., every single aspect of the proposed model is governed by energy minimization. First the kinematics associated with twinning is discussed in Subsection 3.1. Subsequently, the constitutive equations are addressed in Subsection 3.2. The resulting model is presented in Subsection 3.3.

3.1. Kinematics of twinning

In this section, the kinematics associated with deformation-induced twinning is described. In line with James (1981), the deformation between the initial phase and the twinning phase is coupled by a Hadamard-type compatibility condition, i.e., twinning is considered as a certain rank-one convexification (Ortiz and Repetto, 1999; Carstensen et al., 2002). The presented framework is very general and applies also to higher-order laminates. As a matter of fact, second-order laminate structures will be analyzed within the numerical examples. Within each phase showing the original lattice structure, a standard multiplicative decomposition of the deformation gradient is adopted, while an extended decomposition is elaborated for the twinning phase. This extended decomposition accounts for the lattice re-orientation, the shear strain induced by twinning as well as for the deformation history prior to twinning. Since the total deformation associated with the aforementioned laminate structure does not fulfill the Hadamard compatibility condition, an additional boundary layer is introduced. By doing so, a compatible deformation field can be constructed.

3.1.1. Deformation within the initial phase and the twinning phase

Analogously to the crystal plasticity model discussed in Section 2, a multiplicative decomposition of the deformation is adopted. Accordingly, for the deformation of the initial phase without twinning which is highlighted by the superscript $(+)$ in what follows, the standard split

$$\boldsymbol{F}^{+} = \boldsymbol{F}^{\mathrm{e}+} \cdot \boldsymbol{F}^{\mathrm{p}+} \tag{32}$$

is used. By way of contrast, additional deformation modes have to be taken into account in the twinning phase. The first of those is the twinning-induced shear strain a.k.a. intrinsic phase distortion, see e.g., James (1981); Mueller (1999); Aubry et al. (2003). The respective deformation gradient reads

$$\boldsymbol{F}_{\mathrm{Twin}} = \boldsymbol{I} + (\boldsymbol{a} \otimes \boldsymbol{n}) \tag{33}$$

with $\boldsymbol{n}$ ($||\boldsymbol{n}|| = 1$) and $\boldsymbol{a}$ being two vectors corresponding to the twinning plane and the shear direction. The amplitude of twinning $||\boldsymbol{a}||$ is related to the type of crystal lattice. In the case of hcp metals, it is dictated by the crystal axial ratio, i.e., $||\boldsymbol{a}|| = f(c/a)$, see Christian and Mahajan (1995). The second deformation mode which has also to be considered within the twinning phase is the deformation history, e.g., the phase could have already experienced dislocation slip before twinning. Such deformations are represented by the deformation gradient $\boldsymbol{F}_{\mathrm{Hist}}$. Combining the aforementioned deformation modes, the deformation gradients of the different phases are decomposed according to

$$\text{Initial phase before twinning (superscript } +) \; : \quad \boldsymbol{F}^{+} = \boldsymbol{F}^{\mathrm{e}+} \cdot \boldsymbol{F}^{\mathrm{p}+} \tag{34}$$

$$\text{New phase after twinning (superscript } -) \; : \quad \boldsymbol{F}^{-} = \boldsymbol{F}^{\mathrm{e}-} \cdot \boldsymbol{F}^{\mathrm{p}-} \cdot \boldsymbol{F}_{\mathrm{Twin}} \cdot \boldsymbol{F}_{\mathrm{Hist}}. \tag{35}$$

Analogously to classical crystal plasticity theory, the ordering of the different gradients in Eq. (35) has been chosen in line with the deformation chronology. Clearly, even with such a motivation, many questions regarding the multiplicative decomposition of $\boldsymbol{F}$ are still open and controversially discussed in the literature, see, e.g., Xiao et al. (2006) and references cited therein. However, they are far beyond the scope of the present paper. In any case, decompositions of the type (35)

have already been successfully applied to a broad variety of different mechanical problems, cf. Boyce et al. (1992); Levitas (1998); Idesman et al. (2000); Meggyes (2001); Mosler and Bruhns (2009b).

A closer look at Eq. (34) and Eq. (35) reveals that the model has not been completely defined yet. More precisely, the deformation gradient $\boldsymbol{F}_{\mathrm{His}}$ needs further explanation. This variable is strongly related to the interaction between already existing dislocations and twinning. Unfortunately, only little experimental information is available, cf. Kim et al. (2009). Therefore, certain assumptions are required. One such assumption is that the deformation history is completely reset by twinning. In this case, $\boldsymbol{F}_{\mathrm{His}} = \boldsymbol{1}$ and consequently,

$$\boldsymbol{F}^{-} = \boldsymbol{F}^{\mathrm{e}-} \cdot \boldsymbol{F}^{\mathrm{p}-} \cdot \boldsymbol{F}_{\mathrm{Twin}}. \tag{36}$$

Alternatively, one could assume that the dislocation structures is not at all affected by twinning. This implies $\boldsymbol{F}_{\mathrm{His}} = \boldsymbol{F}^{\mathrm{p}+}$ and thus,

$$\boldsymbol{F}^{-} = \boldsymbol{F}^{\mathrm{e}-} \cdot \boldsymbol{F}^{\mathrm{p}-} \cdot \boldsymbol{F}_{\mathrm{Twin}} \cdot \boldsymbol{F}^{\mathrm{p}+}. \tag{37}$$

During deformation of the twinning phase, $\boldsymbol{F}_{\mathrm{His}} = \boldsymbol{F}^{\mathrm{p}+}$ remains constant in this case, cf. Hansen et al. (2010). In the present paper, Eq. (36) is considered, since preliminary molecular dynamical simulations confirm this assumption.

Remark 3. *Since twinning transforms the lattice of the initial phase to a new configuration, it can also affect the elastic properties. However, the elastic anisotropy of magnesium is not very pronounced and the elastic deformation is comparably small. Thus, an isotropic constitutive model is adopted. As a result, the elastic material parameters have been assumed as twinning invariant.*

3.1.2. Compatibility of deformation between the different phases

In the previous section, the deformation within each phase has been decomposed into the physically most relevant parts. However, the deformation gradients in such phases are evidently not completely independent, but they have to fulfill the compatibility condition

$$\boldsymbol{F}^{-} - \boldsymbol{F}^{+} = (\boldsymbol{a} \otimes \boldsymbol{n}). \tag{38}$$

of Hadamard-type, cf. James (1981). Furthermore, the volume average of both gradients has to be identical to their macroscopic counterpart, i.e.,

$$\boldsymbol{F} = (1 - {}_1\xi)\ \boldsymbol{F}^{+} + {}_1\xi\ \boldsymbol{F}^{-}. \tag{39}$$

Here, ${}_1\xi = \mathrm{vol}(\Omega^{-})/\mathrm{vol}(\Omega) \in [0;1]$ is the relative twinning volume and $\Omega := \Omega^{-} \cup \Omega^{+}$. A graphical interpretation of the resulting deformation implied by Eqs. (38) and (39) is shown in Fig. 2. While in the upper part of Fig. 2 a periodic rank-one laminate is illustrated, a second-order laminate is depicted below that figure. Interestingly, such laminates have been observed in many materials, particularly in metals, cf. Mueller (1999); Ortiz and Repetto (1999); Kohn (1991); Pedregal (1993); Ortiz et al. (2000) and references cited therein. According to Fig. 2, twinning can be described by a binary tree structure consisting of leaves and branch joints. Each node of the tree corresponds to the deformation of one laminate $(\boldsymbol{F}^{+}; \boldsymbol{F}^{-})$, while the deformation at the joint of two branches is associated with the volumetric average of the leaves' deformations. The number of branching sequences defines the level of a laminate.

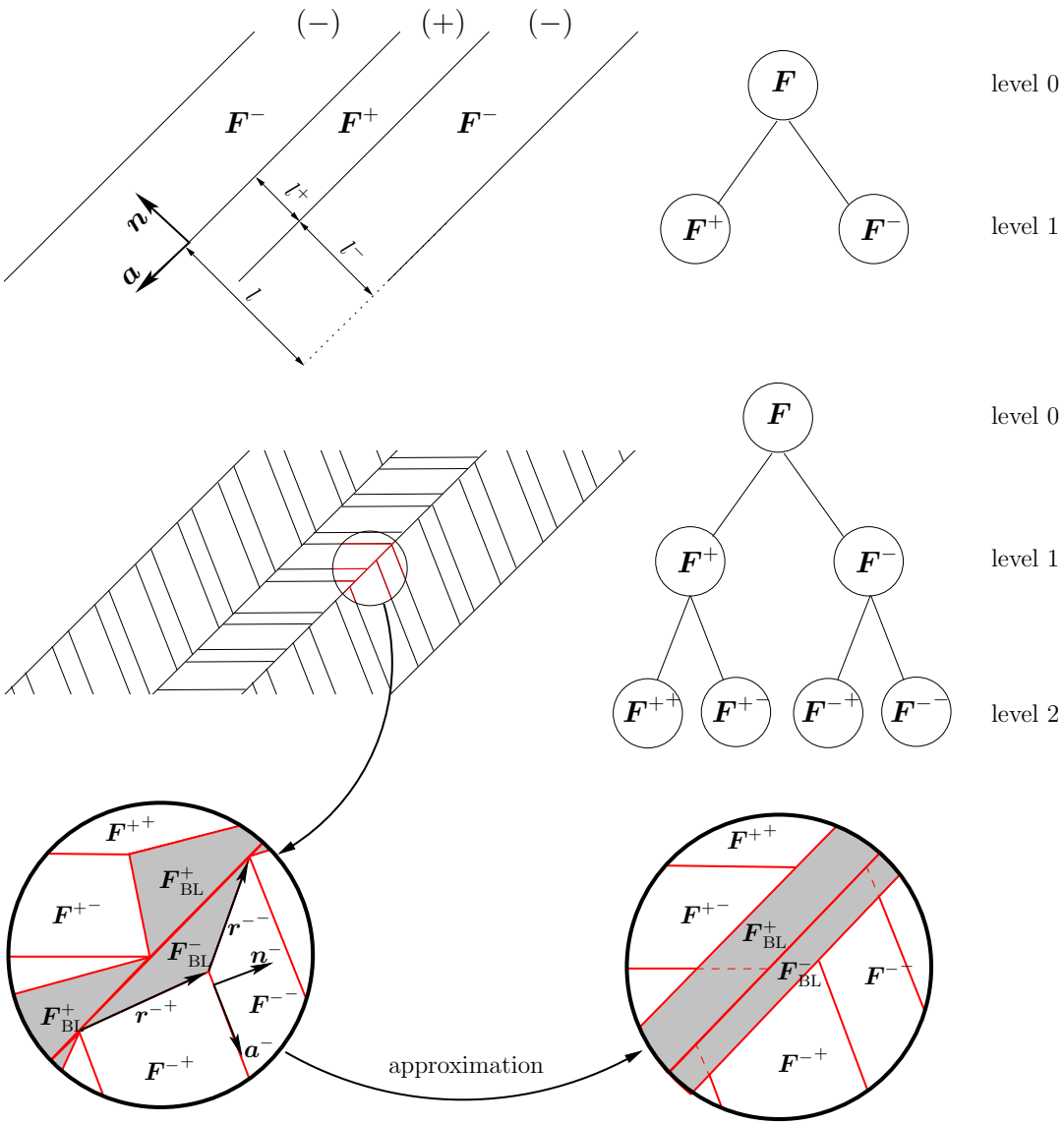

Figure 2: Schematic illustration of sequential laminates and their representative graph of deformation: top: rank-one laminates; middle: rank-two laminates; bottom left: magnification of the boundary layer which is necessary for a continuous deformation; bottom right: approximated boundary layer

Remark 4. *In general, deformation-induced twinning can occur successively by several twinning variants. In this case, the aforementioned phase decomposition model has to be considered several times, see Fig. 2. For highlighting the laminate level, left subscripts will be used (${}_2\xi^-$). Alternatively, the number of superscripts of $\boldsymbol{F}$ shows this level as well. Hence, $\boldsymbol{F}^{+-}$ is a second-order laminate. In this connection, the nth index of $\boldsymbol{F}$ corresponds to the nth phase decomposition.*

3.1.3. Deformation within the boundary layer

The Hadamard compatibility conditions (38) and (39) ensure that the deformation gradients associated with a rank-one laminate results from a continuous deformation. As a consequence and as shown in Fig. 2, the respective laminates fit perfectly together. It is well known that such a compatibility cannot be guaranteed anymore for higher-order laminates. Even if each phase decomposition fulfills the Hadamard compatibility conditions, the resulting deformation is usually not rank-one compatible. This incompatibility gives rise to the formation of boundary layers, i.e., misfits. Following Ortiz et al. (2000), the deformation gradient within such layers can be computed as

$$\boldsymbol{F}^{\pm}_{\mathrm{BL}} = \boldsymbol{F}^{\pm} + \boldsymbol{a}^{\pm} \otimes \boldsymbol{n}^{\pm}_{\mathrm{BL}} \tag{40}$$

with

$$\boldsymbol{n}^{\mp}_{\mathrm{BL}} = ({}_2\xi^{\mp})\ \frac{\boldsymbol{n}^{\mp} \cdot \boldsymbol{r}^{\mp^+}}{|\boldsymbol{r}^{\mp^+}|^2}\boldsymbol{r}^{\mp^+} - (1 - {}_2\xi^{\mp})\ \frac{\boldsymbol{n}^{\mp} \cdot \boldsymbol{r}^{\mp^-}}{|\boldsymbol{r}^{\mp^-}|^2}\boldsymbol{r}^{\mp^-}. \tag{41}$$

In the present paper and following (Stupkiewicz and Petryk, 2002; Petryk et al., 2003; Aubry et al., 2003; Kochmann and Le, 2009), the deformation gradient (40) within the boundary layer is approximated by

$$\boldsymbol{F}^{\pm}_{\mathrm{BL}} = \boldsymbol{F}^{\pm}. \tag{42}$$

Accordingly, the wedge-shaped boundary layer (exact solution) is approximated by a parallelepiped. Evidently, Eq. (42) does not satisfy the Hadamard compatibility condition between the boundary layer and the adjacent leaves. However, if the number of laminates is sufficiently large, the difference between Eq. (40) and Eq. (42) is negligible, i.e., both gradients converge to one another. Experimental confirmation of thin boundary layers in microstructures showing twinning can be found, e.g., in (Appel and Wagner, 1998; Stupkiewicz and Petryk, 2002), see Fig. (3).

3.1.4. Example: Kinematics associated with the channel die test (sample E)

In this section, the kinematics discussed before is specified for the channel die test, cf. Kelley and Hosford (1968). More precisely, the sample labeled as "E" is considered. For this sample, the twinning systems $\{[01\bar{1}1](0\bar{1}12), [0\bar{1}11](01\bar{1}2)\}$ have been observed in the respective experiments. Furthermore, since the Schmid factor of the basal system is zero and the activation energies of prismatic and pyramidal slip are much higher than that of tensile twinning, only tensile twinning is expected to be active. However, twinning reorients the parent crystal lattice about 90 degrees. As a result, it leads to different Schmid factors. For this reason, pyramidal dislocations of the type $\{[11\bar{2}\bar{3}](11\bar{2}2), [\bar{1}\bar{2}\bar{1}\bar{3}](\bar{1}\bar{2}\bar{1}2), [\bar{1}\bar{1}2\bar{3}](\bar{1}\bar{1}22), [1\bar{2}1\bar{3}](1\bar{2}12)\}$ become active within the twinning phase.

Fig. (4) shows the aforementioned microstructure associated with sample "E". Accordingly, it corresponds to a second-order laminate. As discussed before, the second level of such laminates is due to twinning and consequently, the vectors $\boldsymbol{n}$ and $\boldsymbol{a}$ follow directly from crystallographic information, i.e., they are known in advance. By way of contrast, the amplitude of deformation cannot be determined a priori for the laminates of first order. Thus $||\boldsymbol{a}||$ represents an unknown in this case, see Remark 5.

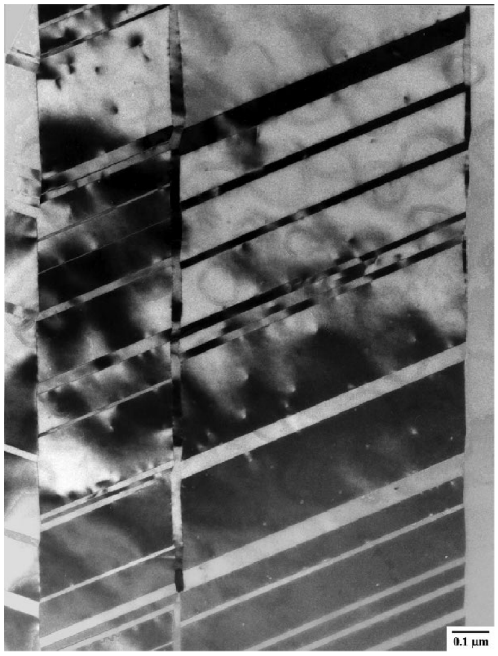

Figure 3: Twinning microstructure in Ti-Al alloy; see Appel and Wagner (1998) (reprint with permission)

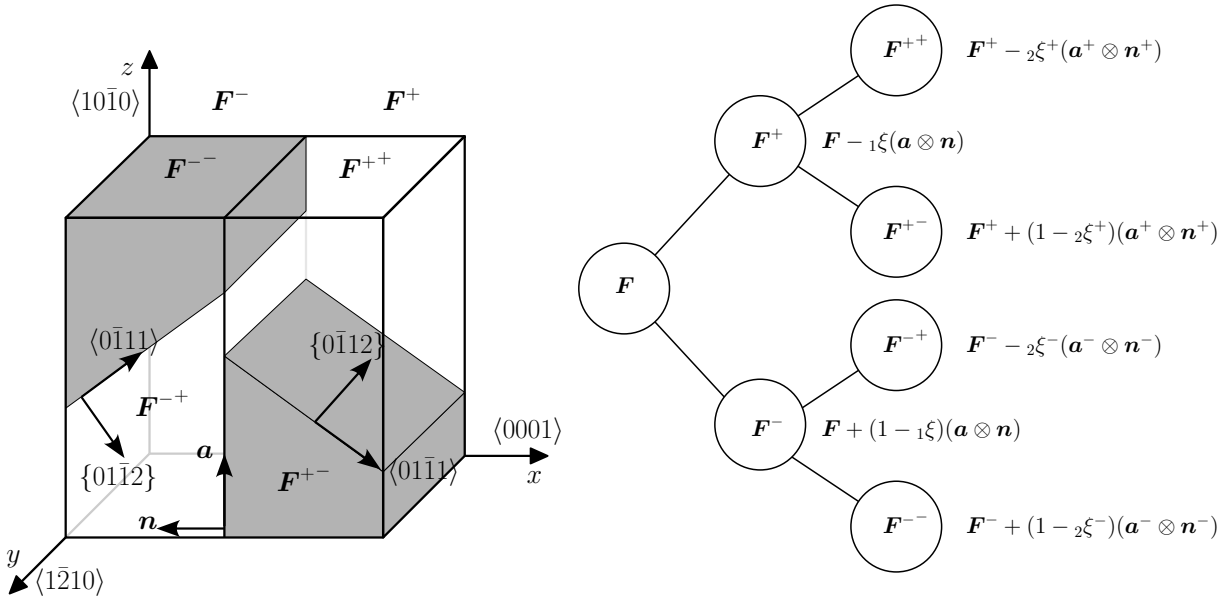

Figure 4: Left: schematic illustration of rank-one twinning laminates in a cubic single crystal sample; right: graph (tree) of the laminates' deformations

By combining the second-order laminate structure shown in Fig. 4 with the dislocation ac-

tivities, the deformations within the different phases can be decomposed as

$$\boldsymbol{F}^{+\,+} = \boldsymbol{F}^{\mathrm{e}+\,+} \quad \text{and} \quad \boldsymbol{F}^{-\,+} = \boldsymbol{F}^{\mathrm{e}-\,+}, \tag{43}$$

$$\boldsymbol{F}^{+\,-} = \boldsymbol{F}^{\mathrm{e}+\,-} \cdot \boldsymbol{F}^{\mathrm{p}+\,-} \cdot \boldsymbol{F}_{\mathrm{Twin}_{\langle 01\bar{1}1\rangle\{0\bar{1}12\}}} \tag{44}$$

and

$$\boldsymbol{F}^{-\,-} = \boldsymbol{F}^{\mathrm{e}-\,-} \cdot \boldsymbol{F}^{\mathrm{p}-\,-} \cdot \boldsymbol{F}_{\mathrm{Twin}_{\langle 0\bar{1}11\rangle\{01\bar{1}2\}}}. \tag{45}$$

As a consequence and in line with experimental observations, a plastic deformation (dislocations) may only occur within the twinning phase. By way of contrast, the initial crystal is fully elastic for sample "E".

For describing nonlocal effects related to the energy of the twinning interface, the number of such interfaces is defined. Neglecting other size effects, the thickness of the laminates is defined by

$$\text{level} \quad 0 \qquad l \;=: \text{ Thickness of the sample} \tag{46}$$

$$\text{level} \quad 1 \qquad {}_1l^{+} \;=\; (1-{}_1\xi)l \quad , \quad {}_1l^{-} \;=\; ({}_1\xi)l \tag{47}$$

$$\text{level} \quad 2 \qquad {}_2l^{+\,+} \;=\; (1-{}_2\xi^{+})\frac{{}_1l^{+}}{{}_2n^{+}} \quad , \quad {}_2l^{+\,-} \;=\; ({}_2\xi^{+})\frac{{}_1l^{+}}{{}_2n^{+}} \tag{48}$$

$$\text{level} \quad 2 \qquad {}_2l^{-\,+} \;=\; (1-{}_2\xi^{-})\frac{{}_1l^{-}}{{}_2n^{-}} \quad , \quad {}_2l^{-\,-} \;=\; ({}_2\xi^{-})\frac{{}_1l^{-}}{{}_2n^{-}} \tag{49}$$

where ${}_2n^{+}$ and ${}_2n^{-}$ indicate the number of laminates of the second level. With such definitions, the thickness of the boundary layer is obtained by using the shear distortion of the twinning laminate (see Fig. 5), i.e.,

$$\begin{aligned} {}_2l^{+}_{\mathrm{BL}} &= \frac{1}{2}\,{}_2\xi^{+}\;\lambda_{\mathrm{Twin}}\;{}_2l^{+\,-} \\ {}_2l^{-}_{\mathrm{BL}} &= \frac{1}{2}\,{}_2\xi^{-}\;\lambda_{\mathrm{Twin}}\;{}_2l^{-\,-} \end{aligned} \tag{50}$$

and the volume fraction of the boundary layer can thus be described as a function of the twinning volume fraction, i.e.,

$${}_2\xi^{\pm}_{\mathrm{BL}} = f({}_2\xi^{\pm}) = \frac{1}{2}\,{}_2\xi^{\pm}\;\lambda_{\mathrm{Twin}}\;\sin(\theta)\;\left({}_2l^{\pm\,-}\right)^2\;\frac{w}{\mathrm{vol}(\Omega)}. \tag{51}$$

Here, w and θ are the width of the respective sample and the angle between the twinning interface and the rank-one laminate. According to Fig. (5), a boundary layer has only considered at the center of the specimen, cf. Kochmann and Le (2009).

Remark 5. *In general, the microstructure (order of laminate and its orientations), together with its induced deformation, is intrinsically unknown and thus, it has to be computed. As shown in the next section, it follows from minimizing the stress power of the respective solids, i.e., the energetically most favorable microstructures will form. Fortunately, due to the relatively simple boundary conditions and experimental observations, many variables can be a priori determined for sample "E" (see also Aubry et al. (2003)). For an overview, the variables defining the microstructure are summarized in Tab. 2.*

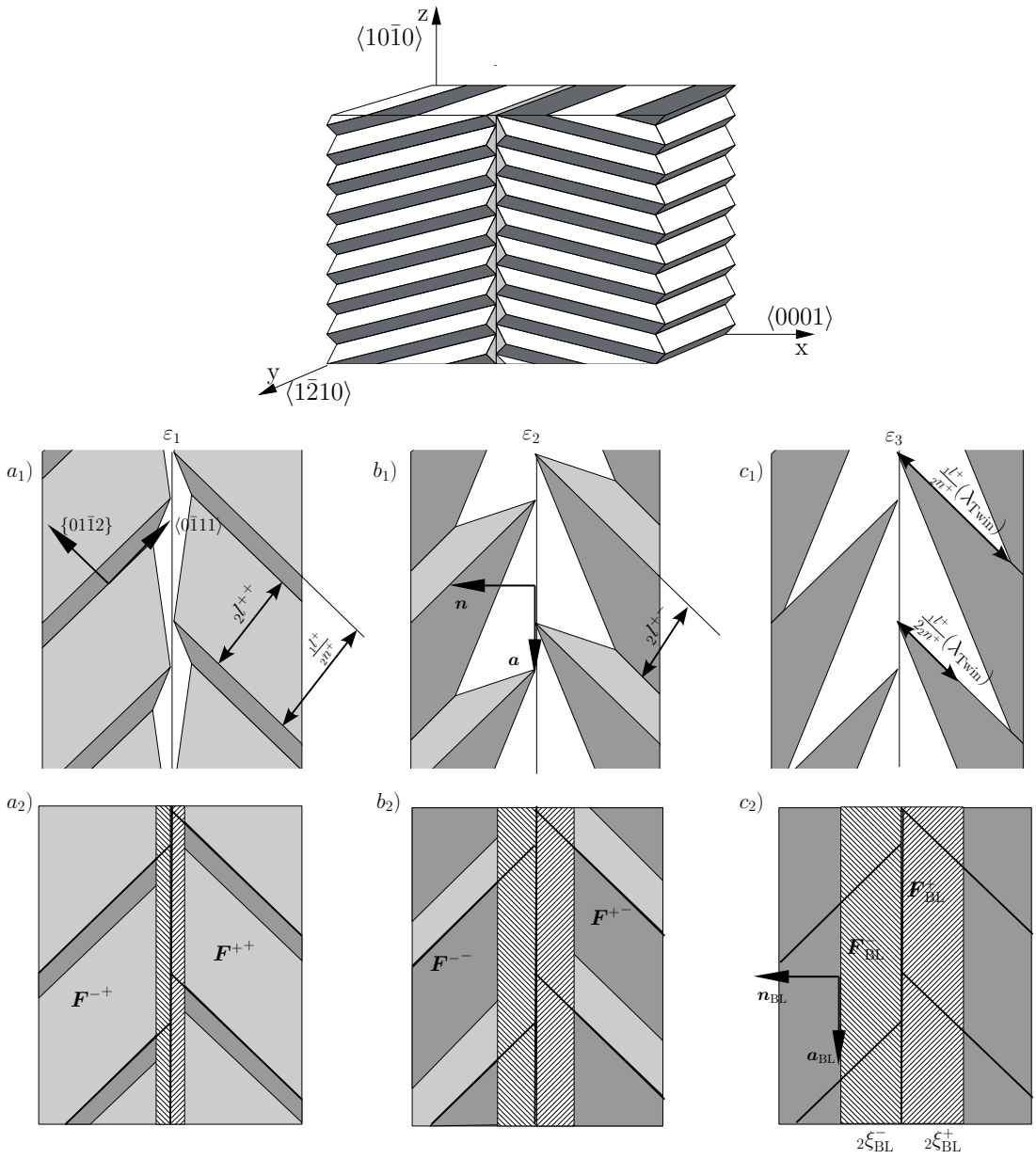

Figure 5: Schematic illustration of twinning evolution by means of rank-one laminates for monotonic loading (strain amplitudes: $\varepsilon_1 < \varepsilon_2 < \varepsilon_3$): Due to the misfit between higher-order laminates, wedge-shaped boundary layers are necessary for a continuous deformation (upper figure). They are approximated by a straight boundary layer (bottom figure).

3.2. Constitutive equations

Having discussed the kinematics associated with dislocation slip and deformation-induced twinning, focus is now on the constitutive equations. First, the Helmholtz energy is elaborated in Subsection 3.2.1. Subsequently, the dissipation related to twinning is addressed in Subsection 3.2.2. The final model is summarized in Subsection 3.3 and numerical aspects concerning its implementation are also given. In line with the crystal plasticity model shown in Section 2,

Table 2: List of microstructure related variables

$_1\xi$	$_2\xi^+ = {}_2\xi^-$	$_2\xi^+_{\mathrm{BL}} = {}_2\xi^-_{\mathrm{BL}}$	$_2n^+_{\mathrm{int}} = {}_2n^-_{\mathrm{int}}$	l	$_1l^+ = {}_1l^-$	$_2l^{++} = {}_2l^{-+}$	$_2l^{+-} = {}_2l^{--}$
0.5	unknown	Eq. (51)	unknown	12.7 mm	$l/2$	unknown	unknown

	$\boldsymbol{a}$	$\boldsymbol{n}$	$\boldsymbol{a}^+$	$\boldsymbol{n}^+$	$\boldsymbol{a}^-$	$\boldsymbol{n}^-$
direction	$\langle\bar{1}010\rangle$	$\{000\bar{1}\}$	$\langle01\bar{1}1\rangle$	$\{0\bar{1}12\}$	$\langle0\bar{1}11\rangle$	$\{01\bar{1}2\}$
amplitude	unknown	1	0.35	1	0.35	1

it is uniquely driven by energy minimization.

3.2.1. Helmholtz energy

Helmholtz energy within the different phases. Within each phase, the deformation may be purely elastic or elastoplastic as a result of dislocations. Accordingly and following Section 2, a Helmholtz energy of the type

$$\Psi = \Psi^{\mathrm{e}}(\boldsymbol{C}^{\mathrm{e}}) + \Psi^{\mathrm{p}}(\boldsymbol{\lambda}) \tag{52}$$

represents a suitable choice. As in the previous section, the elastic response is approximated by the neo-Hooke-type model (28), while the stored energy due to plastic work is again decomposed into self hardening and latent hardening effects, i.e.,

$$\Psi^{\mathrm{p}} = \Psi^{\mathrm{p}}(\boldsymbol{\lambda}) = \Psi^{\mathrm{p}}_{\mathrm{self}}(\boldsymbol{\lambda}) + \Psi^{\mathrm{p}}_{\mathrm{lat}}(\boldsymbol{\lambda}). \tag{53}$$

A size-dependence of the hardening parameters can be accounted for by assuming that Ψ^{p} depends also on the mean free path of dislocations, cf. Aubry et al. (2003); Hansen et al. (2010), i.e.,

$$\Psi^{\mathrm{p}} = \Psi^{\mathrm{p}}(\boldsymbol{\lambda}, \boldsymbol{h}) \tag{54}$$

with $\boldsymbol{h} = \{h^{(1)}, \dots h^{(n)}\}$ containing the mean free path of the n different dislocation systems. However, due to lack of experimental observation, such an enhanced model will not be used within the numerical examples presented in the next section. A size-effect of Hall-Petch-type will nevertheless be implemented by relating the yield limit $\Sigma_0^{(a)}$ to the mean free path of dislocations, cf. Eq. (58).

Helmholtz energy associated with the twinning interface. According to experimental measurements, the energy of twinning interfaces is relatively small compared to the elastic energy stored within the bulk, see Ball and James (1987); Morris et al. (2005). For instance, the interface energy reported in Morris et al. (2005) is about $k = 0.140$ mJ/m^2. Based on this measurement, the total energy of n_{int} interfaces showing a cross sectional area of A_{int} each is computed as

$$\Psi_{\mathrm{mix}}(n_{\mathrm{int}}, A_{\mathrm{ini}}) = k n_{\mathrm{int}} A_{\mathrm{int}}. \tag{55}$$

Clearly, a constant area specific energy is a comparably simple assumption. However, due to lack of experimental information, it seems to be appropriate. Furthermore and equally importantly, the presented constitutive framework is very general and allows also the incorporation of more complicated interface models.

Helmholtz energy associated with the boundary layer. Unfortunately, even less information is available about the boundary layer. More precisely, only the respective deformation gradient is known (see Eq. (40)). For this reason, a fully elastic response is assumed, i.e.,

$$\Psi_{\mathrm{BL}} = \Psi_{\mathrm{BL}}(\boldsymbol{C}). \tag{56}$$

In the numerical examples, the neo-Hooke-type model (28) is adopted. However, it bears emphasis that any elastoplastic model can easily be included as well.

Total Helmholtz energy. By summarizing the different Helmholtz energies introduced before, the total stored energy of a first-order laminate can be computed as

$$\begin{aligned}\Psi = (1-\xi_{\mathrm{BL}})\left((1-\xi)\Psi^{+}(\boldsymbol{C}^{+},\boldsymbol{\lambda}^{+}) + \xi\ \Psi^{-}(\boldsymbol{C}^{-},\boldsymbol{\lambda}^{-})\right)\\ + \xi_{\mathrm{BL}}\ \Psi_{\mathrm{BL}}(\boldsymbol{C}_{\mathrm{BL}}) + \Psi_{\mathrm{mix}}(n_{\mathrm{int}}, A_{\mathrm{int}}).\end{aligned} \tag{57}$$

Since the Helmholtz energy is an extensive variable, it decomposes additively. Although the Helmholtz energy has been specified here only for a first-order laminate, it can be generalized in a straightforward manner to the more general case. For that purpose, Eq. (57) has to be applied recursively. Further details are omitted here. However, they will be discussed in Subsection 3.3.

3.2.2. Dissipation and kinetics

Dissipation due to plastic deformation – dislocations within the different phases. Analogously to Section 2, dissipation due to plastic deformation is modeled by a functional being positively homogeneous of degree one. Consequently and fully identical to Section 2,

$$\mathcal{D} = \sum_{a=1}^{n} \zeta^{(a)}\ \Sigma_0^{(a)} \geq 0. \tag{58}$$

is considered. However and in sharp contrast to Section 2, a size-effect of Hall-Petch-type is accounted for. For this reason, the critical effective resolved shear stress $\tilde{\Sigma}_0$ is related to the mean free path of dislocations according to

$$\tilde{\Sigma}_0 = \Sigma_0 + \frac{T}{bh} \tag{59}$$

with h being the length of this path, b and T denoting material parameters (amplitude of the Burgers' vector and line tension) and Σ_0 representing the resolved shear stress of the local model (without Hall-Petch effect). Thus, the smaller this length, the higher the resolved shear stress Σ_0. Within the numerical simulations, the thickness of the laminates is taken as h.

Dissipation due to twinning nucleation. Analogously to dislocation slip, initiation of twinning lenticulars is also accommodated by elementary dislocations, see Christian and Mahajan (1995). Thus, a dissipation functional similar to Eq. (58) represents a suitable choice. Considering one active slip system and neglecting hardening effects, Eq. (58) can be re-written as

$$\zeta^{(a)}\ \Sigma_0^{(a)} = \zeta^{(a)}\ |\boldsymbol{\Sigma} : \left(\boldsymbol{s}^{(a)} \otimes \boldsymbol{m}^{(a)}\right)|. \tag{60}$$

As a result, a dissipation potential of the type

$$\mathcal{D}_{\text{int}} = \mu\, \hat{\epsilon}\, \dot{n}_{\text{int}} \left(\boldsymbol{\Sigma} : (\boldsymbol{a} \otimes \boldsymbol{n}) \right), \tag{61}$$

seems to be well suited for describing the kinetics associated with twinning nucleation. Here, $\hat{\epsilon}$ is a material parameter. It bears emphasis that twinning is a polar deformation system and thus, twinning initiation requires a positive resolved shear stress, see Christian and Mahajan (1995). Therefore and in contrast to Eq. (60), the sign of the driving force $(\boldsymbol{\Sigma} : (\boldsymbol{a} \otimes \boldsymbol{n}))$ is important. For instance, already existing twinning laminates can be annihilated under negative resolved shear stress ($\dot{n} < 0$). This is called de-twinning. Accordingly, n is not necessarily monotonically increasing and thus, the physical constraint $n \geq 0$ has to be carefully checked.

Dissipation due to propagation of twinning interfaces. Similarly to twinning initiation, zonal dislocations are again the underling physical mechanism associated with twinning propagation, see Christian and Mahajan (1995). Thus, the evolution equation governing such phenomena can be derived in line with those of ideal dislocation slip. Accordingly, the rate of twinning growth is assumed to be proportional to zonal dislocation slip, i.e.,

$$\xi \propto \frac{n_{\text{zd}}}{\hat{n}_{\text{zd}}} \tag{62}$$

where n_{zd} and $\hat{n}_{\text{zd}}$ are the current number of zonal dislocations and the total number of zonal dislocations required for transforming the volume of the initial phase completely into the reoriented twinning phase. As a results, the total energy dissipation due to twinning propagation denoted as $\mathcal{D}_\xi$ can be formally written as

$$\int_{t_n}^{t_{n+1}} \mathcal{D}_\xi \, \mathrm{d}t \propto \Delta\xi \propto \Delta n_{\text{zd}}. \tag{63}$$

Hence, the analogy between twinning propagation caused by zonal dislocations and dislocation slip suggests to use a dissipation functional being positively homogeneous of degree one in ξ. Summarizing this similarity and having in mind that the twinning volume can also decrease, a dissipation functional of the type

$$\mathcal{D}_\xi = \mu\, \epsilon\, \dot{\xi} \ (\boldsymbol{\Sigma} : (\boldsymbol{a} \otimes \boldsymbol{n})) \tag{64}$$

represents a physically sound choice. In Eq. (64), μ and ϵ are the elastic shear modulus and an additional material parameter, see Kochmann and Le (2009); Levitas and Ozsoy (2009). Analogously to twinning initiation, twinning propagation does also depend on the loading direction. More precisely, Eq. (64), together with the dissipation inequality $\mathcal{D}_\xi \geq 0$, leads to twinning or de-twinning depending on the sign of the driving force $\boldsymbol{\Sigma} : (\boldsymbol{a} \otimes \boldsymbol{n})$.

Total dissipation. By combining the different dissipative mechanisms analyzed within the previous paragraphs and accounting for the extensivity of energy, the total dissipation reads thus

$$\mathcal{D}_{\text{total}} = \underbrace{(1 - \xi_{\text{BL}}) \left((1 - \xi)\mathcal{D}^+ + \xi\, \mathcal{D}^- \right)}_{=:\, \mathcal{D}_{\text{dis}}} + \mathcal{D}_\xi + \mathcal{D}_{\text{int}}. \tag{65}$$

Accordingly, it consists of a term related to dislocation slip ($\mathcal{D}_{\text{dis}}$), a term associated with twinning initiation ($\mathcal{D}_{\text{int}}$) and a dissipation corresponding to twinning propagation ($\mathcal{D}_{\xi}$). Note that $\mathcal{D}_{\text{dis}}$ has the same structure as the Helmholtz energy of the bulk (compare $\mathcal{D}_{\text{dis}}$ to the first line in Eq. (57)).

3.3. The resulting non-local model for deformation-induced twinning – variational constitutive updates

In Section 2, standard crystal plasticity theory was recast into an equivalent variational principle. They key idea was the minimization of the stress power. The same method is also applied here. For that purpose, the stress power

$$\mathcal{E} = \dot{\Psi} + \mathcal{D}_{\text{total}} \tag{66}$$

is integrated over the time interval $[t_n; t_{n+1}]$ yielding the incrementally defined potential

$$I_{\text{inc}} = \int_{t_n}^{t_{n+1}} \{\dot{\Psi} + \mathcal{D}\} \, \mathrm{d}t = I_{\text{inc}}(\boldsymbol{F}, \boldsymbol{\lambda}^-, \boldsymbol{\lambda}^+, \xi, \xi_{\text{BL}}(\xi), n_{\text{int}}, \boldsymbol{a}, \boldsymbol{n}). \tag{67}$$

Here, a first-order laminate has been considered for the sake of simplicity. According to Eq. (67) and analogously to crystal plasticity, the functional depends on the macroscopic strains through $\boldsymbol{F}$ and on the internal variables related to dislocation slip ($\boldsymbol{\lambda}^{\pm}$). However, it is also affected by the microstructure ($\xi, \xi_{\text{BL}}(\xi), n_{\text{int}}, \boldsymbol{a}, \boldsymbol{n}$). As mentioned in Remark 5, some of the microstructural parameters can be a priori computed for certain boundary value problems (e.g., due to symmetry). Based on Eq. (67), the unknowns are computed from the optimization problem

$$(\boldsymbol{\lambda}^-, \boldsymbol{\lambda}^+, \xi, \xi_{\text{BL}}(\xi), n_{\text{int}}, \boldsymbol{a}, \boldsymbol{n}) = \arg \inf_{\boldsymbol{\lambda}^{\pm}, \xi, \xi_{\text{BL}}(\xi), n_{\text{int}}, \boldsymbol{a}, \boldsymbol{n}} I_{\text{inc}} \tag{68}$$

and the stresses follow subsequently from

$$\boldsymbol{P} = \partial_{\boldsymbol{F}} \left(\inf_{\boldsymbol{\lambda}^{\pm}, \xi, \xi_{\text{BL}}(\xi), n_{\text{int}}, \boldsymbol{a}, \boldsymbol{n}} I_{\text{inc}} \right). \tag{69}$$

A careful analysis of Eqs. (66) and (67), together with the Helmholtz energy (57) and the dissipation functional (65), reveals that minimization principle (68) is indeed physically sound. More explicitly, stationarity of I_{inc} with respect to the internal variables $\boldsymbol{\lambda}^{\pm}$ is equivalent to enforcing the yield functions, i.e., $\phi^{(a)} \leq 0$. This can be seen by noticing that the structure of the dissipation (65) and that of the Helmholtz energy (57) is identical for all terms involving $\boldsymbol{\lambda}^{\pm}$. As a result, except for a factor c, this stationarity condition is equivalent to that of standard crystal plasticity, i.e.,

$$\partial_{\boldsymbol{\lambda}^+} I_{\text{inc}} = \partial_{\boldsymbol{\lambda}^+} \left\{ \underbrace{(1 - \xi_{\text{BL}})\, \xi}_{=c} \underbrace{\left[\Psi^+_{n+1} + \sum_{a=1}^{n} \Delta\zeta^{(a)} \, \Sigma_0^{(a)} \right]}_{\text{crystal plasticity}} \right\}. \tag{70}$$

Furthermore and as already pointed out in Ortiz et al. (2000), stability of I_{inc} with respect to the microstructural parameters $\boldsymbol{a}$, ξ and $\boldsymbol{n}$ is equivalent to traction equilibrium, configurational torque equilibrium and configurational force equilibrium at the internal interfaces, respectively. The final optimality condition with respect to the number of laminates can be physically interpreted as a balance condition between surface and bulk energies.

Based on recursively applying Eq. (67), the incrementally defined potential I_{inc} can also be derived for higher-order laminates. For instance, the second-order laminate analyzed within the next section is given by

$$I_{\text{inc}} = (1 - {}_1\xi_{\text{BL}}) \left[(1 - {}_1\xi) I^{+}_{\text{inc}} + {}_1\xi \; I^{-}_{\text{inc}}\right] + (1 - {}_1\xi_{\text{BL}}) \int_{t_n}^{t_{n+1}} {}_1\left\{\mathcal{D}_{\xi} + \mathcal{D}_{\text{int}}\right\} \, \mathrm{d}t + \int_{t_n}^{t_{n+1}} {}_1\xi_{\text{BL}} \; \Psi_{\text{BL}} \, \mathrm{d}t. \tag{71}$$

Here, the first term is simply the volume average of the energies related to the first-order laminates, the second one is associated with dissipation due to twinning and the third terms corresponds to the boundary layer. Focusing on second-order laminates the energies $I^{\pm}_{\text{inc}}$ are given by Eq. (67).

Remark 6. *For computing the incrementally defined potential I_{inc} (see Eq. (67)) a fully implicit time integration scheme is applied. While a classical backward Euler scheme is adopted for the scalar-value variables, the exponential mapping is used for integrating the flow rule, see Eq. (21).*

4. Numerical results and discussion

In this section, the novel model suitable for the prediction of the microstructure in magnesium is carefully analyzed by comparing experimental observations to numerically obtained results. For that purpose, the channel die test with the crystal orientation labeled as "E" is considered. A detailed description of the test and the induced mechanisms has already been given in Subsection 3.1.4. According to Subsection 3.1.4, the resulting deformation is approximated by a second-order laminate. The a priori known as well as the unknown parameters describing the respective microstructure are summarized in Tab. 2. For highlighting the features of the model advocated in the present paper, three different constitutive models are adopted. They are summarized below.

- Local model: size effects are excluded by neglecting the boundary layer and by fixing the number of laminates for each phase, i.e.,

$$ {}_2\xi^{\pm}_{\text{BL}} = 0, \quad {}_2n^{\pm} = 1. \tag{72}$$

- Non-local, dislocation-free model: dislocations within the different phases are completely neglected, i.e.,

$$ {}_2\boldsymbol{\lambda}^{\pm} = 0, \quad \boldsymbol{F}^{\pm\pm} = \boldsymbol{F}^{\mathrm{e}\pm\pm}, \quad \boldsymbol{F}^{\mathrm{p}\pm\pm} = \boldsymbol{I}. \tag{73}$$

- Fully non-local model including dislocation slip

Table 3: Material parameters used in the numerical analysis

Elastic Properties	$\lambda_{\mathrm{E}} = 34$(GPa)		$\mu = 17$ (GPa)	
Hardening parameters: Pyramidal system				
Σ_0 (MPa)	h_0 (MPa)	Σ_∞ (MPa)	l^{ab}	b (nm)
25	7100	105	25	6
Twinning related material parameters				
λ_{Twin}	ϵ	$\hat{\epsilon}$	k (mJ/m^2)	T (N)
0.35	2×10^{-4}	2×10^{-4}	0.140	0.03×10^{-9}

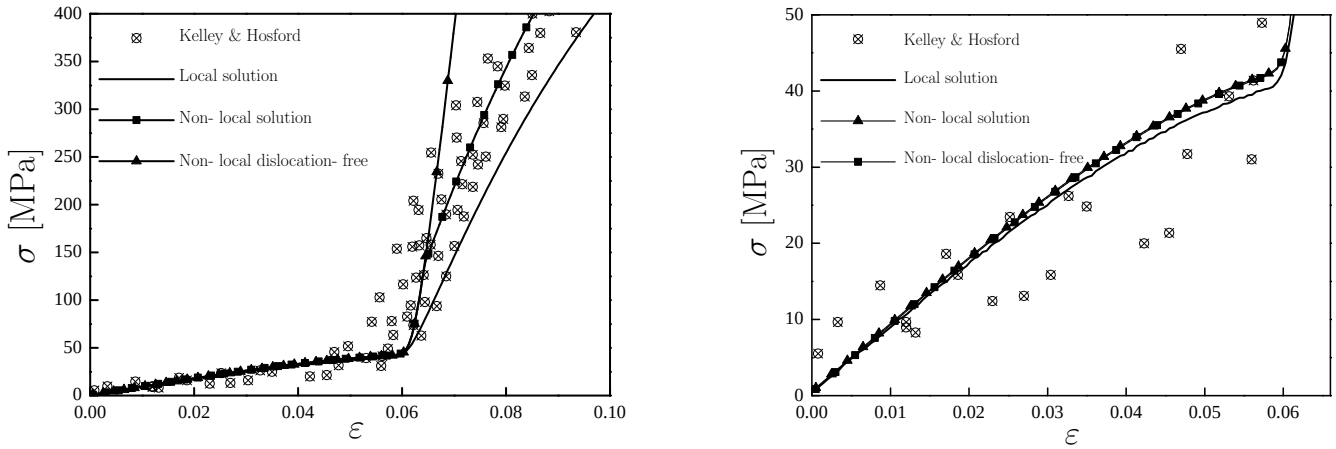

Figure 6: Channel die experiment (see Kelley and Hosford (1968)): comparison between experimentally measured data and computed stress-strain response. The right figure represents a zoom in of that on the left hand side. Within the diagrams, the true stress vs. the true strain has been plotted.

The material parameters used within the different models are given in Tab. 3. By comparing Tab. 3 to Fig. 1, one can see that the parameters describing the elastoplastic response of the respective solids have not been changed.

The stress response as predicted by the different models, together with the experimentally measured data (see Kelley and Hosford (1968)), is shown in Fig. 6. While the left figure covers the whole loading range, a zoom in of the first loading stage is depicted on the right hand side. This magnification reveals that the difference between the models is only minor until the twinning phase becomes more dominant. More precisely, the mechanical response is predicted as slightly stiffer, if the boundary layer and the interface energy are taken into account. The small increase in stiffness is due to the relatively low area specific energy k. The evolution of the twinning volume fractions ${}_{\{1,2\}}\xi^{\pm}$ is illustrated in Fig. 7. Accordingly, the first loading stage is associated with a transformation of the initial phase to the twinning phase. When the twinning process is completed, the new phase becomes active, resulting in a significant macroscopic hardening effect (see $\varepsilon > 0.06$ in Fig. 6). As evident in Fig. 6, all models capture this transition very well. However, the non-local disclocation-free model overpredicts the stiffness of the twinning phase. Contrariwise, the solid is predicted as too weak, if the crystal is allowed to further relax by

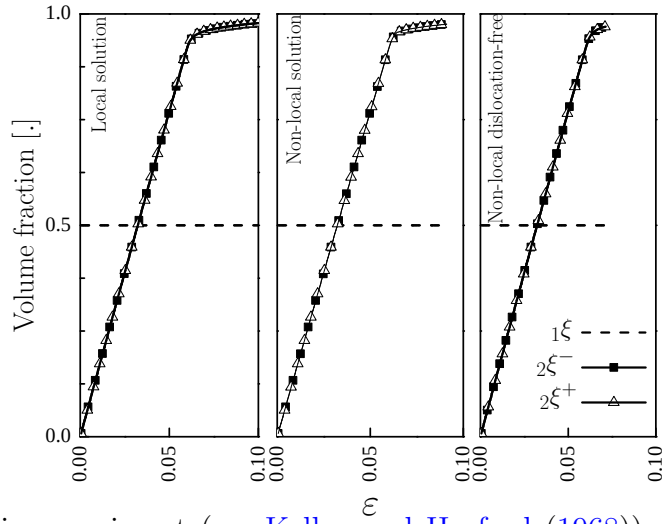

Figure 7: Channel die experiment (see Kelley and Hosford (1968)): evolution of the twinning volume fraction

neglecting the boundary layer. The best stress-strain response is obtained for the fully non-local model taking also dislocation-related hardening effects into account.

It bears emphasis that the analyzed example is relatively simple, e.g., monotonic, radial loading. Consequently, unrealistic elastic unloading as predicted by the non-local model without dislocation slip cannot be seen. Furthermore, since only one specimen size is investigated in Kelley and Hosford (1968) and the interface energy is relatively low, the difference between the local model and its non-local extension is relatively small. A key difference between the local model and its non-local extension can nevertheless be seen in Fig. 8. This figure shows the number of laminates during loading. Clearly, this number cannot be computed by means of a purely local theory. According to Fig. 8, the total number of laminates ($_2n^+ + {}_2n^-$) reaches 7000 at $\varepsilon_{zz} = 0.06$. Considering the initial size of the single crystal (see Kelley and Hosford (1968)) as well as the evolution of the twinning volume fractions ${}_{\{1,2\}}\xi^{\pm}$, the thickness of such laminates can be computed, see Fig. 8. As evident from Fig. 8, the model leads to thick laminates during the early stages of deformation. For the analyzed example, this thickness decreases monotonically. Beyond $\varepsilon = 0.06$, the microstructure consists of very fine laminates ($< 3\mu$m) and more than 97% of the volume has been transformed to the twinning phase, cf. Fig. 7. Similar trends were also reported, e.g., in Hansen et al. (2010).

5. Conclusion

In the present paper, an incremental energy principle suitable for the analysis of the deformation systems in hcp metals such as magnesium has been presented. Based on lamination theory, the proposed method naturally avoids the decomposition of the twinning history into so-called pseudo-dislocations followed by a reorientation of the total crystal. By way of contrast, the proposed model captures the transformation of the crystal lattice due to twinning in a continuous fashion by simultaneously taking dislocation slip within both, possibly co-existent,

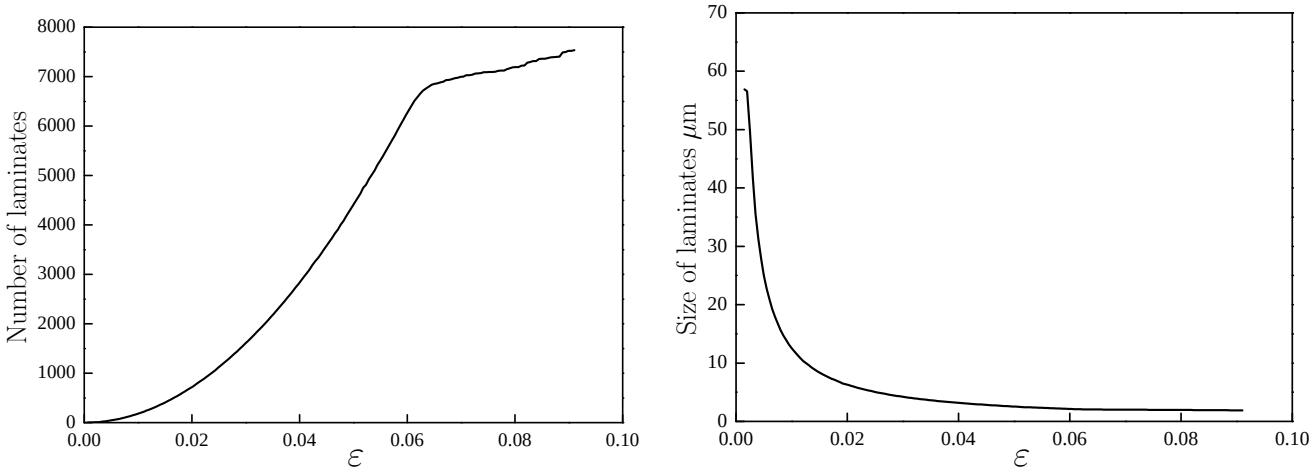

Figure 8: Channel die experiment (see Kelley and Hosford (1968)): left: evolution of the number of laminates of the second level (${}_2n^+ + {}_2n^-$); right: numerically predicted size of the rank-two laminates layers

phases into account – as observed in experiments. The shear strain imposed by twinning as well as the deformation history were consistently included within the twinned domain by an enhanced multiplicative decomposition of the deformation gradient. Furthermore and in sharp contrast to previous models suitable for the analysis of the deformation systems in magnesium, the Helmholtz energy of the twinning interfaces and that of the boundary layer necessary for fulfilling the boundary conditions were explicitly considered. Analogously, the energy due to twinning nucleation and that related to twinning growth were also accounted for by suitable dissipation functionals. By doing so, the plastic deformation due to dislocations, the total volume of the twinning phase as well as the number of twin lammellas represented the unknowns to be computed within the resulting energy principle. Consequently, the thickness of the lamellas can be computed as well. By interpreting this thickness as the mean free path of dislocations, a size effect of Hall-Petch-type was naturally included within the novel model. Although the predictive capabilities of the final approach were only demonstrated for magnesium by analyzing the channel die test, the presented approach is very general and thus, it can also be applied to other materials showing twin lamellas, e.g., titanium aluminides.

6. Acknowledgment

The authors gratefully acknowledge the support of W. Hosford for providing the primary data of his pioneering experimental work on single crystal magnesium.

7. References

Agnew, S. R., Duygulu, Ö., 2005. Plastic anisotropy and the role of non-basal slip in magnesium alloy AZ31B. International Journal of Plasticity (21), 1161–1193.

Ando, S., Tonda, H., 2000. Non-basal slip in magnesium-lithium alloy single crystals. Material Transactions 41, 1188–1191.

Appel, F., Wagner, R., 1998. Microstructure and deformation of two-phase γ-titanium aliminides. Materials Science and Engineering 22, 187–268.

Aubry, S., Fago, M., Ortiz, M., 2003. A constrained sequential-lamination algorithm for the simulation of sub-grid microstructure in martensitic materials. Computer Methods in Applied Mechanics and Engineering 192, 2823–2843.

Aubry, S., Ortiz, M., 2003. The mechanics of deformation-induced subgrain-dislocation structures in metallic crystals at large strains. Proceeding of the Royal Society 459, 3131–3158.

Ball, J. M., James, R. D., 1987. Fine phase mixtures as minimizers of energy. Archive for Rational Mechanics and Analysis 100, 13–52.

Blawert, C., Manova, D., Störmer, M., Gerlach, J., Dietzel, W., Mändl, S., 2008. Correlation between texture and corrosion properties of magnesium coatings produced by pvd. Surface and Coatings Technology 202 (11), 2236–2240, protective Coatings and Thin Films 07, E-MRS Spring Meeting.

Boyce, M. C., Montagut, E. L., Argon, A. S., 1992. The effects of thermomechanical coupling on the cold drawing process of glassy polymers. Polymer Engineering & Science 32, 1073–1085.

Carstensen, C., Hackl, K., Mielke, A., 2002. Non-convex potentials and microstructures in finite-strain plasticity. Proceeding of the Royal Society A 458, 299–317.

Christian, J. W., Mahajan, S., 1995. Deformation twinning. Progress in Materials Science 39, 1–157.

Coleman, B. D., 1964. Thermodynamics of materials with memory. Archive for Rational Mechanics and Analysis 17, 1–45.

Ericksen, J. L., 1979. On the symmetry of deformable crystals. Archive for Rational Mechanics and Analysis 72, 1–13.

Graff, S., Brocks, W., Steglich, D., 2007. Yielding of magnesium: From single crystal to polycrystalline aggregates. International Journal of Plasticity 23, 1957–1978.

Hackl, K., Fischer, F. D., 2008. On the relation between the principle of maximum dissipation and inelastic evolution given by dissipation potentials. Proceeding of the Royal Society A 464, 117–132.

Hansen, B. L., Bronkhorst, C. A., Ortiz, M., 2010. Dislocation subgrain structure and modeling the plastic hardening of metallic single crystals. Modelling and Simulation in Materials Science and Engineering 18, 1–42.

Hauser, F. E., Starr, C. D., Tietz, L., Dorn, J. E., 1955. Deformation mechanisms in polycrystalline aggregates of magnesium. Transactions of the ASM 47, 102–134.

Hill, R., 1972. On constitutive macro-variables for heterogeneous solids at finite strain. Proceedings of the Royal Society 326, 131–147.

Homayonifar, M., Mosler, J., 2010. On the coupling of plastic slip and deformation-induced twinning in magnesium: A variationally consistent approach based on energy minimization. International Journal of PlasticityDOI: 10.1016/j.ijplas.2010.10.009.

Idesman, A. V., Levitas, V. I., Stein, E., 2000. Structural changes in elastoplastic material: a unified finite-element approach to phase transformation, twinning and fracture. International Journal of Plasticity 16, 893–949.

James, R. D., 1981. Finite deformation by mechanical twinning. Archive for Rational Mechanics and Analysis 77, 143–176.

James, R. D., Hane, K. F., 2000. Martensitic transformations and shape-memory materials. Acta Materialia 48, 197–222.

Kalidindi, S. R., 2001. Modeling anisotropic strain hardening and deformation textures in low stacking fault energy fcc metals. International Journal of Plasticity (17), 837–860.

Kelley, E. W., Hosford, W. F., 1968. Plane-strain compression of magnesium and magnesium alloy crystals. Transactions of the Metallurgical Society of AIME 242, 654–661.

Khan, A. S., Pandey, A., Gnäupel-Herold, T., Mishra, R. K., 2010. Mechanical response and texture evolution of az31 alloy at large strains for different strain rates and temperatures. International Journal of Plasticity InPress, DOI: 10.1016/j.ijplas.2010.08.009.

Kim, G. S., Yi, S., Huang, Y., Lilleodden, E., 2009. Twining and slip activity in magnesium $< 11\bar{2}0 >$ single crystal. In: Mechanical Behavior at Small Scales – Experiments and Modeling. Vol. 1224 of MRS Proceedings.

Kochmann, D. M., Le, K. C., 2008. Dislocation pile-ups in bicrystals within continuum dislocation theory. International Journal of Plasticity (24), 2125–2147.

Kochmann, D. M., Le, K. C., 2009. A continuum model for initiation and evolution of deformation twinning. Journal of the Mechanics and Physics of Solids 57, 987–1002.

Kohn, R. V., 1991. The relaxation of a double-well energy. Continuum Mechanics and Thermodynamics 3, 193–236.

Lee, E. H., 1969. Elastic-plastic deformations at finite strains. ASME, Journal of Applied Mechanics 36, 1–6.

Levitas, V. I., 1998. Thermomechanical theory of martensitic phase transformations in inelastic materials. International Journal of Solids and Structures 35, 889–940.

Levitas, V. I., Ozsoy, I. B., 2009. Micromechanical modeling of stress-induced phase transformations. part 1. thermodynamics and kinetics of coupled interface propagation and reorientation. International Journal of Plasticity 25, 239–280.

Lilleodden, E., 2010. Microcompression study of Mg (0001) single crystal. Scripta Materialia 62, 532–535.

Lion, A., 2000. Constitutive modelling in finite thermoviscoplasticity: a physical approach based on nonlinear rheological models. International Journal of Plasticity 16, 469–494.

Mandel, J., 1972. Plasticite Classique et Viscoplasticite. Cours and Lectures au CISM No. 97, International Center for Mechanical Science. Springer-Verlag, New York.

Meggyes, A., 2001. Multiple decomposition in finite deformation theory. Acta Mechanica 146, 169–182.

Miehe, C., 2002. Strain-driven homogenization of inelastic microstructures and composites based on an incremental variational formulation. International Journal for Numerical Methods in Engineering 55, 1285–1322.

Miehe, C., Lambrecht, M., 2003. A two-scale finite element relaxation analysis of shear bands in non-convex inelastic solids: small-strain theory for standard dissipative materials. International Journal for Numerical Methods in Engineering 58, 1–41.

Mielke, A., Theil, F., I., L. V., 2002. A variational formulation of rate-independent phase transformations using an extremum principle. Archive for rational mechanics and analysis 162, 137–177.

Mordike, B. L., Ebert, T., 2001. Magnesium: Properties - applications - potential. Materials Science and Engineering A 302, 37–45.

Morris, J. R., Ye, Z., Yoo, M. H., 2005. First-principles examination of the twin boundary in hcp metals. Philosophical Magazine 85 (2), 233–238.

Mosler, J., Bruhns, O. T., 2009a. On the implementation of variational constitutive updates at finite strain. In: Hackl, K. (Ed.), Variational Concepts with Application to the Mechanics of Materials. Springer, in press.

Mosler, J., Bruhns, O. T., 2009b. Towards variational constitutive updates for non-associative plasticity models at finite strain: models based on a volumetric-deviatoric split. International Journal of Solids and Structures 49, 1676–1685.

Mosler, J., Cirak, F., 2009. A variational formulation for finite deformation wrinkling analysis of inelastic membranes. Computer Methods in Applied Mechanics and Engineering 198, 2087–2098.

Mueller, S., 1999. Variational models for microstructure and phase transitions. Calculus of Variations and Geometric Evolution Problems 1713, 85–210.

Nebebe, M., Stutz, L., Bohlen, J., Steglich, D., Letzig, D., Mosler, J., 2009. Exprimental measurement and constitutive model for forming process of magnesium alloy sheet. In: Kainer, K. (Ed.), Magnesium-8th International Conference on Magnesium Alloys and their Application. pp. 764–770.

Obara, T., Yoshinga, H., Morozumi, S., 1973. {11-22} {-1-123} slip system in magnesium. Acta Metallurgica 21, 845–853.

Ortiz, M., Repetto, E. A., 1999. Nonconvex energy minimization and dislocation structures in ductile single crystals. Journal of the Mechanics and Physics of Solids 47, 397–462.

Ortiz, M., Repetto, E. A., Stainier, L., 2000. A theory of subgrain dislocation structures. Journal of the Mechanics and Physics of Solids 48, 2077–2114.

Ortiz, M., Stainier, L., 1999. The variational formulation of viscoplastic constitutive updates. Computer Methods in Applied Mechanics and Engineering 171, 419–444.

Pedregal, P., 1993. Laminates and microstructure. European Journal of Applied Mathematics 4, 121–149.

Petryk, H., Fischer, F. D., Marketz, W., Clemens, H., Appel, F., 2003. An energy approach to the formation of twins in tial. Metallurgical and Materials Transactions 34, 2827–2836.

Pitteri, M., 1985. On the kinematics of mechanical twinning in crystals. Archive for Rational Mechanics and Analysis 88, 25–57.

Proust, G., Tome, C. N., Jain, A., Agnew, S. R., 2009. Modeling the effect of twinning and detwinning during strain-path changes of magnesium alloy az31. International Journal of Plasticity 25, 861–880.

Rasmussen, K., Pedersen, O., 1980. Fatigue of copper polycrystals at low plastic strain amplitudes. Acta Metallurgica 28, 1467–1478.

Reed-Hill, R. E., Robertson, W. D., 1957. Deformation of magnesium single crystals by nonbasal slip. Journal of Metals - Transactions AIME 220, 496–502.

Rice, J. R., 1971. Inelastic constitutive relations for solids: an internal variable theory and its application to metal plasticity. Journal of the Mechanics and Physics of Solids 19, 433–455.

Roberts, E., Partridge, P. G., 1966. The accomodation around $\{10\bar{1}2\}\langle\bar{1}011\rangle$ twins in magnesium. Acta Metallurgica 14, 513–527.

Roters, F., Eisenlohr, P., Hantcherli, L., Tjahjanto, D. D., Bieler, T. R. R. D., 2010. Overview of constitutive laws, kinematics, homogenization and multiscale methods in crystal plasticity finite-element modeling: Theory, experiments, applications. Acta Materiala 58, 1152–1211.

Simha, N. K., 1997. Twin and habit plane microstructures due to the tetragonal to monoclinic transformation of zirconia. Journal of the Mechanics and Physics of Solids 45, 261–263.

Staroselsky, A., Anand, L., 2003. A constitutive model for hcp materials deforming by slip and twinning: application to magnesium alloy az31b. International Journal of Plasticity 19, 1843–1864.

Stupkiewicz, S., Petryk, H., 2002. Modelling of laminated microstructures in stress-induced martensitic transformations. Journal of the Mechanics and Physics of Solids 50, 2303–2331.

Tegart, W. J. M., 1964. Independent slip systems and ductility of hexagonal polycrystals. Philosophical Magazine 9, 339–341.

Van Houtte, P., 1978. Simulation of the rolling and shear texture of brass by the taylor theory adapted for mechanical twinning. Acta Metallurgica 26, 591–604.

Wonsiewicz, B. C., Backofen, W. A., 1967. Independent slip systems and ductility of hexagonal polycrystals. Transaction of Metallurgical Soc. AIME 239, 1422–1433.

Xiao, H., Bruhns, O. T., Meyers, A., 2006. Elastoplasticity beyond small deformations. Acta Mechanica 182, 31–111.

Yoshinaga, H., Horiuchi, R., 1963. On the nonbasal slip in magnesium crystals. Transactions of the Japan Institute of Metals 5, 14–21.